Catalysis Science & Technology

Accepted Manuscript

ROYAL SOCIETY OF CHEMISTRY

www.rsc.org/catalysis

The highly dispersed Cu nanoparticles as an efficient catalyst for the synthesis of biofuel 2-methylfuran

Fang Dong [a,b], Guoqiang Ding [c], Hongyan Zheng [c], Xiaoming Xiang [a,b], Linfeng Chen [c], Yulei Zhu [a,c,*], Yongwang Li [a,c]

[a] *State Key Laboratory of Coal Conversion, Institute of Coal Chemistry, Chinese Academy of Sciences, Taiyuan 030001, PR China*

[b] *Graduate University of Chinese Academy of Sciences, Beijing 100039, PR China*

[c] *Synfuels China Co., Ltd., Beijing 101407, PR China*

[*]Corresponding author: *State Key Laboratory of Coal Conversion, Institute of Coal Chemistry, Chinese Academy of Sciences, Taiyuan 030001, PR China.* Tel.: +86 351 7117097; fax: +86 351 7560668.

E-mail address: zhuyulei@sxicc.ac.cn (Y. Zhu).

Abstract

Cu/SiO_2 catalysts were synthesized by the different methods, which greatly influenced their texture and the catalytic performance. AE-Cu/SiO_2 catalyst was prepared by the ammonia evaporation method and showed a 95.5% yield to 2-methylfuran (as a promising fuel additive) because of the cooperative effect of surface Cu^0, Cu^+ species and acid sites, which respectively stemmed from the reduction of highly dispersed CuO species, copper species fiercely interacted with support SiO_2 and the especial structure. The ammonia evaporation method was favorable to the conformation of copper phyllosilicate phase with the lamellar structure, which could provide a large number of Cu nanoparticles and acid sites and further improve the activity and selectivity. Crucially, the stability of AE-Cu/SiO_2 catalyst (> 210 h) was also significantly improved due to the enhanced interaction of copper-silicon, which could immobilize copper particles and resist the fast transmigration (aggregation and loss) of copper particles in the thermal treatment process. On the contrary, CP-Cu/SiO_2 catalyst was synthesized by the conventional precipitation method and presented the poor activity and stability to 2-methylfuran because of the large copper particles, the severe aggregation and loss of copper species during reaction. Compared with the conventional CP-Cu/SiO_2 catalyst, the use of AE-Cu/SiO_2 catalyst in the synthesis of biofuel 2-methylfuran could not only improve the yield of desire product, but also decrease at least a 20 °C of reaction temperature which is propitious to prolong the lifetime of Cu/SiO_2 catalyst.

Keywords: Biomass conversion, furfural, hydrogenolysis, copper catalysts, 2-methylfuran

1. Introduction

The selective conversion of biomass and biomass derivatives has become one of the main ways to obtain chemicals and fuels in relieving the fossil energy and environment crisis [1]. Fortunately, biomass is the plentiful renewable resource in the world, which is chiefly derived from the catalytic conversion of agriculture and forestry residues, and the source is very wide and economical [2, 3]. Therefore, the development and use of biomass resources are vitally important for the remission of fossil energy crisis, and the effective use of a large number of surplus biomass resources.

Currently, a central challenge of biomass conversion lies in developing an environmental efficiently catalyst and green process for the manufacture of high added-value fuels and chemicals [4, 5]. For example, the selective conversion of biomass derived furfural has become a hot research project in both industry and academia. Furfural is a promising lignocelluosic material manufactured about at the rate of 20 million tons per year by the dehydration of hemicelluloses such as xylose and arabinose, and has greatly attracted attention as a potential C5 resource for the synthesis of chemicals [6, 7]. Furfural with two special functional groups (C=C and C=O groups) has been considered as a representative compound for researching the selective conversion of C=C and C=O groups [8, 9]. Typically, furfural conversion includes a series of reactions such as the hydrogenation and hydrogenolysis of C=O groups, the hydrogenation of C=C groups from furan ring, the selective breaking of C-C bands, the polymerization of intermolecular and so on [10]. Especially, the reduction of furfural in H_2 over the supported metal catalysts is a fundamental reaction to convert into the oxygen-containing compounds, including furfuryl alcohol (FOL), tetrahydrofurfuryl alcohol (THFOL), 2-methylfuran (2-MF) and 2-methyltetrahydrofuran (2-MTHF), which are marketable as specialty oxygen-containing chemicals. Especially, the hydrogenation and hydrogenolysis of side substituents -CH=O groups to produce 2-methylfuran is a well-known reaction [9, 10]. 2-MF with oxygen atom could enhance combustion performance of fuel, and it has been treated as a promising fuel additive on the basis of good combustion performance and high octane value (RON=103) [11, 12]. 2-MF is significantly derived from the conversion of furfural and FOL via various catalysts, optimally Cu-based catalysts [12, 13, 14, 15]. Because Cu-based

catalysts are the excellent activity and low cost for the conversion of -CH=O groups, and are relatively ineffective for the conversion of C=C groups [16].

For the first time, Adkins et al. [17] reported the reduction of furfural in H_2 over a Cu/Cr catalyst. The hydrogenation of furfural in liquid phase was carried out for 11.5 h at 100°C and 10-15 MPa pressure (H_2), and the low yield of 2-MF was obtained. In the industry, the catalyst used in furfural hydrogenation is a Cu/Cr catalyst modified with different additives [18]. However, the critical shortage for the containing-chromium catalysts is toxicity which causes the human health crisis and the severe environmental pollution [19, 20]. After that, Zhu et al. [21] reported an efficient synthesis of 2-MF and GBL over Cr-free Cu-based catalysts from furfural and 1,4-butanediol at 240°C. S. Sitthisa et al. [22] and Zheng et al. [23] also reported that the hydrogenation-hydrogenolysis of furfural to 2-MF was performed on Cu/SiO_2 catalyst, and the desire product was 2-MF. More recently, Ke Xiong et al. [24] discovered that molybdenum carbide could be treated as a novel deoxygenation catalyst for the synthesis of 2-MF, but a low yield of 2-MF was discovered. Interestingly, among the multifarious catalysts, Cu/SiO_2 has been extensively studied and used in many reactions owing to the high activity, low cost and green benefit, especially the hydrogenation of dimethyl oxalate and the hydrogenolysis of glycerol [25, 26, 27, 28]. However, the key challenge for commercialization lies in the poor stability of Cu/SiO_2 catalyst due to the severe aggregation at high temperature, which spontaneously limited its application in the industry. Herein, it is a high expectation to develop a stable efficiently catalyst for the industrial application.

In our previous work, Cu/SiO_2 catalyst exhibited the superior catalytic performance in furfural hydrogenation than Cu/Al_2O_3 and Cu/ZnO catalysts [29]. The reason of the superior performance for Cu/SiO_2 catalyst was notably attributed to the synergistic effect of metal and acid site. In order to synthesize the highly active and stable Cu/SiO_2 catalyst for the commercial application, we further investigated the effect of the preparation method. Generally, the highly dispersed metal particles on the ideal support not only enhanced the activity of catalysts, but the stability could be evidently improved. More significantly, the high dispersion also decreased the amount of metal compound and further advanced the reuse efficiency of catalysts as a result of the trivial loss of metal constituents. Gong et al. [30] reported that the big surface area of catalysts was realized by the special morphology, which could induce the production of highly

dispersed metal nanoparticles and advance the activity in the synthesis of ethanol from dimethyl oxalate hydrogenation. This reaction requires the hydrogenation and hydrogenolysis of C=O/C-O groups, which is similar to the synthesis of 2-MF through furfural conversion. The synthesis of 2-MF involves the hydrogenation of -CH=O groups in furfural molecular and the further hydrogenolysis of -CH_2-OH groups in the intermediate FOL (Scheme 1). Therefore, the design and synthesis of big surface area and high metal dispersion catalysts play the important roles in improving the yield and stability of desire product 2-MF via furfural conversion.

In this work, we have successfully synthetized a highly efficient Cu/SiO_2 catalyst via the improvement of preparation method. The enhancement of activity and stability for Cu/SiO_2 catalyst was observed with respect to furfural hydrogenation. In order to further explore the relationships of structure-performance, the samples were also systemically analyzed by various characterizations, such as BET, N_2O chemisorption, XRD, FT-IR, Raman, and TEM techniques. Besides, we also investigated the deactivation of conventional Cu/SiO_2 catalyst because of an obvious decrease of 2-MF selectivity after reaction about 112 h, and the results verified that the main reason of deactivation was the obvious transmigration (aggregation and loss) of copper species during reaction.

To the best of our knowledge, this article is the first report about the using of copper phyllosilicate (AE-Cu/SiO_2 sample) in the synthesis of biofuel 2-MF. It is also the first detailed investigation about the difference of catalyst texture, structure and surface properties for the conventional Cu/SiO_2 catalyst (CP-Cu/SiO_2) and copper phyllosilicate (AE-Cu/SiO_2). It is discovered that AE-Cu/SiO_2 catalyst presented the superior activity and stability for the synthesis of 2-MF than the conventional CP-Cu/SiO_2 catalyst. In particular, AE-Cu/SiO_2 catalyst would induce the formation of Cu nanoparticles, which greatly improve the catalytic activity. The lamellar structure of copper phyllosilicate phase could greatly enhance the acid sites of catalyst surface (the production of Cu^+ species), which could promote the hydrogenolysis of -CH_2-OH groups in the intermediate FOL and further improve 2-MF selectivity. More importantly, the enhanced interaction of copper-silicon in AE-Cu/SiO_2 catalyst is favorable to immobilize copper particles on the support surface and resist the transmigration of copper species in the thermal treatment process.

2. Experimental

2.1. Catalyst preparation

CP-Cu/SiO_2 sample was synthetized by the conventional precipitation method [31]. At first, 45.3g of $Cu(NO_3)_2.3H_2O$ was dissolved in the deionized water. Then 116.67g of silica sol (SW-30) mixed with the aqueous solution of $Cu(NO_3)_2$. Afterward, under the vigorous stir, the mixed copper-silicon solution and 1M NH_4HCO_3 aqueous solution were concurrently dropped into 200 mL deionized water. In drop process, the pH value of mixed solution was kept in the range of 6.0-7.0, and the obtained slurry was further aged for 1.0 h. Then the suspension was washed with deionized water for 3-5 times and filtered. After this, the precipitant in air was dried at 120 ºC for 24 h. Subsequently, the obtained precursor was calcined at 450 ºC for 5 h in static air. Finally, CP-Cu/SiO_2 precursor was obtained (Scheme 1).

AE-Cu/SiO_2 sample was synthesized by the ammonia evaporation method [25，30]. Firstly, the 45.3g of $Cu(NO_3)_2.3H_2O$ was dissolved in the deionized water. Then 116.67g of silica sol (SW-30) mixed with the aqueous solution of $Cu(NO_3)_2$ under vigorous stirring. Subsequently, a 25% aqueous solution of ammonia was appended into the mixed copper-silicon solution until pH=12, and then the mixed solution heated to form a gel at 90 °C. After that, the gel was aged at 90 °C until pH=6.0-7.0, further filtrated, washed and dried with the same method as CP-Cu/SiO_2 sample. After dry, the powder was calcined at 450 °C in static air for 5h, and following AE-Cu/SiO_2 precursor was formed (Scheme 1).

2.2. Catalyst characterization

N_2 adsorption-desorption isotherms were operated at -196 ºC with an ASAP 2420 (Micromeritics, Inc). Before N_2 adsorption, the samples were degassed in vacuum at 90 °C for 1 h and 350 °C for 8 h. After that, the Brunauer-Emmett-Teller (BET) surface area (S_{BET}), pore volume (V_p), and average pore size (d_p) of samples were obtained.

The elemental analysis was performed on Optima2100DV, PerkinEl-mer to determine the metal loadings.

N_2O adsorption was performed on Auto Chem. II2920 (Mircromeritics, USA). At first, the samples were loaded into a U-shaped quartz tube. Then the samples were reduced with H_2-TPR

procedure, which would be detailedly described in the following section (H_2-temperature programmed reduction). The copper dispersion and surface area are determined by the dissociation of N_2O adsorption (Supporting information).

X-ray diffraction analysis of samples was recorded with a BrukerAxs D8 diffractometer with Cu Kα radiation (λ=0.154 nm) at 30 kV and 10 mA with a scanning angle (2ɵ) in the range of 10º-80º. The crystallite size of copper was calculated according to Scherrer equation.

TEM was performed on a JEM-2100F high-resolution transmission. The samples are treated by grinding, subsequent dispersing the powder in ethanol and dropping the dilute suspension on copper grids. Typically, the amorphous carbon films were filled into the copper grids.

The IR spectra in the range of 400 - 4000 cm^{-1} were recorded with a Vertex 70 (Bruker) FT-IR spectrophotometer. The determined power samples were mixed with a 2 wt. % KBr. After that, the mixed power at room temperature was quantified and pressed into translucent disks.

Raman patterns were conducted with a LabRAM HR800 system equipped with a CCD detector. The excitation source was the 325 nm of the He–Cd laser with a power of 30 MW. In order to avoid damaging the sample, the system used a 60% reduction of laser output.

In order to investigate the reducibility of samples, H_2-temperature programmed reduction was conducted with Auto Chem. II2920 (Mircromeritics, USA). Prior to test, the samples were loaded into a quartz tube and reduced with a 5 vol% H_2/He mixture (50 $cm^3.min^{-1}$) in the range of 40-400 °C (a heating rate of 5 °C /min). TCD apparatus was used to record the single in the system. A 2-propanol-liquid nitrogen slurry (−89 °C) cooled trap was used to cool the water, which was formed in the reduced process.

Temperature programmed desorption of NH_3 (NH_3-TPD) was implemented with the same instrument as H_2-TPR. In order to clean the moisture and some impurity gases, the samples were cleansed about 2 h in He gas at 400 ºC. Then the samples were cooled and absorbed with NH_3 until saturation. Afterward, the sample was cleansed again with He gas to remove the physically adsorbed NH_3. Hereafter, the sample was heated to 600 ºC at a rate of 5 ºC/min and the desorption of NH_3 was recorded with MS (Agilent). In order to avoid the interference of H_2O, ion current of m/z = 16 was considered as a credible parameters to assess the acidity.

X-ray photoelectron spectroscopy (XPS) was performed on a Physical Electronics PHI 5700 spectrometer. A Mg Ka (1253.6 eV) X-ray source and a multichannel detector were used in this system. In order to further distinguish the Cu^0 and Cu^+ species, Auger electron spectroscopy (XAES) were performed on the samples. Before test, the samples were reduced in

situ with pure H_2 gas (50 mL/min).

2.3. Activity tests and analysis method

Activity tests of the samples were executed in a stainless steel fixed bed reactor (i.d. 12 mm, length 600 mm). Initially, the samples (20-40 mesh) were filled into the isothermal region of the reactor tube, and then samples at 270 °C were adequately reduced with a 5 vol. % H_2/N_2 mixture gas. The distilled furfural was continually brought into an evaporator by HPLC pump after reduction. Afterward, H_2 was introduced into the system through mass flow controller, and furfural was mixed with pure H_2 at the top of preheater. Finally, the mixed reactants were introduced into the fixed-bed reactor.

The liquid products were collected in a gas-liquid separator with a condenser, and analyzed by an off-line gas chromatography (GC6890, Agilent, USA). A capillary column (polyethandiol, 30m×0.32 mm) and a flame ionization detector were used in the system. Another, the tail gas was also determined by an on-line gas chromatography (GC6890, Agilent, USA), which is comprised of a FID detector and a polyethandiol capillary column. A GC-MS (6890N, Agilent, USA) was employed to identify the part products in this system. The carbon balance was better than 96% and the error was about ±3%. Furfural conversion, products selectivity and the carbon balance were calculated according to the following equations:

$$\text{Conversion}\ (\%) = \frac{\text{Amount of furfural converted (mol)}}{\text{Total amount of furfural fed (mol)}} \times 100$$

$$\text{Selectivity}\ (\%) = \frac{\text{Amount of per product produced (mol)}}{\text{Amount of furfural converted (mol)}} \times 100$$

$$\text{Carbon balance}\ (\%) = \frac{\text{Amount of the overall carbon fed (mol)}}{\text{Amount of the overall carbon outflowed (mol)}} \times 100$$

3. Results and Discussion

3.1. Characterization of the catalysts

3.1.1. The texture properties of the catalysts

In order to explore the textural properties of two Cu/SiO_2 samples, N_2 adsorption-desorption isotherms of samples were showed in Table 1 and Fig. 1. Obviously, the S_{BET} (BET surface area) and average pore volume were completely different, and the S_{BET} of

AE-Cu/SiO_2 sample is about three times that of CP-Cu/SiO_2 sample. In addition, AE-Cu/SiO_2 sample has a bimodal pore size distribution, while CP-Cu/SiO_2 sample has only one pore. The average pore diameter of CP-Cu/SiO_2 sample is much bigger than that of AE-Cu/SiO_2 sample. For CP-Cu/SiO_2 sample, the obvious decrease of S_{BET} and pore volume might be related to the block of pore that resulted from the aggregation of copper particles [32]. Copper loadings determined by ICP-OES analysis were almost close to these two samples in Table 1. Additionally, the dissociative N_2O chemisorption of samples was done to determine copper dispersion and specific surface area. The ammonia evaporation method greatly improved copper dispersion and decreased the particles size, which could be instrumental in retarding the sintering of copper particles and escaping the heat during the thermal treatment process. Compared with the conventional Cu/SiO_2 samples, AE-Cu/SiO_2 sample afforded higher copper dispersion and smaller particles size.

Van der Grift et al. [33] proposed that the S_{BET} of catalysts would increase with the increase of copper loading due to the production of more copper phyllosilicate in the urea hydrolysis process. The former literatures [33, 34] also reported that the urea hydrolysis and the selective adsorption of Cu^{2+} ions on the silicon surface could obtain copper phyllosilicate phase. In this work, copper phyllosilicate phase could be synthesized via the ammonia evaporation method. Dramatically, it was observed the appearance of blue color on AE-Cu/SiO_2 sample after calcination, while CP-Cu/SiO_2 sample commonly exhibited dark color in Fig S1, indicating the emergence of some different copper species. F. Zaccheria et al. [35] reported that the existence of CuO species commonly exhibited black color with the large copper particles, while blue color was related to the formation of very small copper particles.

Fig. 2A displays the XRD patterns of Cu/SiO_2 catalysts after drying at 120 °C. CP-Cu/SiO_2 catalyst exhibited the typical X-ray diffractograms of $Cu_2CO_3(OH)_2$, with characteristic diffraction peaks at 14.8°, 17.6°, 24.1°, 31.5° and 35.7° (PDF#41-1390). Interestingly, AE-Cu/SiO_2 catalyst exhibited the typical X-ray diffractograms of $Cu_2Si_2O_5(OH)_2$, with characteristic diffraction peaks at 19.9°, 21.8°, 30.8° , 35.0° , 57.5°and 62.4° (PDF#27-0188). These weak and broad diffraction peaks of AE-Cu/SiO_2 catalyst at 30.8° and 35.0° suggested the existence of copper phyllosilicate phase with weak crystallinity [30]. Additionally, Fig 2B exhibits the XRD patterns of the calcined Cu/SiO_2 catalysts at 450 °C.

The feature peak at 2ɵ of around 20.5° was attributed to amorphous silica [36]. Evident diffraction peaks of CuO at 35.6° and 38.7° (PDF#48-1548) were seen on CP-Cu/SiO_2 catalyst, suggesting the existence of large CuO particles, and the CuO crystallite size is 8.45 nm on the basis of the Scherrer equation. Unexpectedly, the XRD pattern of the calcined AE-Cu/SiO_2 catalyst was virtually identical with that of the dry AE-Cu/SiO_2 catalyst, and no diffraction peak of CuO was observed on the calcined AE-Cu/SiO_2 sample at 450°C. The copper crystallite size of AE-Cu/SiO_2 catalyst was too small to calculate the particles size according to the Scherrer equation. Generally, the particles size below 4 nm cannot be detected by XRD technique [37]. The XRD patterns of two Cu/SiO_2 catalysts suggested that copper species was completely different after calcination: the calcined CP-Cu/SiO_2 catalyst contains a large amount of CuO species, which is derived from the calcination of $Cu_2CO_3(OH)_2$; while the calcined AE-Cu/SiO_2 catalyst mainly exists in the form of $Cu_2Si_2O_5(OH)_2$, which is formed in the precipitation process, and the structure is still not damage after calcination at 450°C.

XRD patterns of the reduced samples were also investigated to explore the existence of copper species. Evidently, the XRD diffraction peaks of CuO species vanished in CP-Cu/SiO_2 catalyst, while three salient peaks emerged at around 43.2°, 50.4°, and 74.1°, indicating the production of metallic Cu [38]. Especially, a diffraction peak of Cu at 43.2 ° was observed on CP-Cu/SiO_2 catalyst (Fig. 2C), and the average size of copper particles is about 14.9 nm according to the Scherrer equation. For AE-Cu/SiO_2 catalyst, the diffraction peak of Cu at 43.2° is obviously weaker and broader than CP-Cu/SiO_2 catalyst, indicating that copper particles of AE-Cu/SiO_2 catalyst were still highly dispersed on silicon surface after reduction. Notably, the reduced AE-Cu/SiO_2 catalyst also exhibited a weak peak at 37.1°, which was attributed to the production of Cu^+ species due to the enhanced interaction of copper-silicon. This interaction is favorable to stable copper particles and resist the fast aggregation.

A great difference was clearly observed on the morphology of two Cu/SiO_2 samples in Fig. 3. Interestingly, CP-Cu/SiO_2 catalyst (Fig. 3a)) obviously exhibited a large number of the spherical CuO particles, while AE-Cu/SiO_2 catalyst (Fig. 3b)) revealed the filandrous morphology which was attributed to copper phyllosilicate phase [25]. Copper phyllosilicate is composed by the special lamellar structure, which was formed via the competitive reaction of Cu^{2+} ions with the silanol and amino groups in the preparation process [38, 39]. Compared with

TEM images before and after the calcination, it was discovered that the lamellar structure was formed in the precipitation process, and the structure is still intact after the calcination at high temperature. Furthermore, the particles size of Cu/SiO_2 catalysts after the reduction was counted in Fig. $3a_3$ and $3b_3$. Copper species of AE-Cu/SiO_2 catalyst were highly dispersed on SiO_2 surface, and produced small Cu nanoparticles about 5 nm. However, the particles size of CP-Cu/SiO_2 catalyst was about three times that of AE-Cu/SiO_2 catalyst after the reduction, further indicating the severe sintering of copper species during the precipitation process.

3.1.2. Structural properties of the catalysts

In order to discriminate the structure information of Cu/SiO_2 catalysts, FTIR spectra as the most convincing characterization of copper phyllosilicate phase were conducted (Fig. 4). Evidently, CP-Cu/SiO_2 catalyst showed two main characteristic bands at 1125 and 800 cm^{-1}, respectively, related to the asymmetric and symmetric stretching of ν_{SiO} bond in the amorphous SiO_2 [25, 30]. Compared with the pure SiO_2, the characteristic peaks of ν_{SiO} bond at 1125 and 800 cm^{-1} completely exhibited and hardly changed in CP-Cu/SiO_2 catalyst, indicating the weak interaction between CuO and SiO_2, also in good agreement with the Raman results (Fig. 5). However, AE-Cu/SiO_2 catalyst presented two characteristic peaks at 670 and 1040 cm^{-1}, revealing that the structure property was substantially different with SiO_2 and CP-Cu/SiO_2. The vibration modes of δ_{OH} bands exhibited the peak at 670 cm^{-1}, while the feature peak at 1040 cm^{-1} was ascribed to the vibration of ν_{SiO} bonds in copper phyllosilicate [30]. Obviously, AE-Cu/SiO_2 sample emerged the largest peak at 670 cm^{-1} due to the existence of a large number of hydroxyl groups, which were caused by the formation of copper phyllosilicate/the lamellar structure. On the other hand, the ν_{SiO} symmetric stretching peak of AE-Cu/SiO_2 sample obviously decreased at 800 cm^{-1}, which also verified the existence of copper phyllosilicate phase. FTIR results suggested that the ammonia evaporation method was propitious to form copper phyllosilicate phase. Additionally, the production of copper phyllosilicate phase was also confirmed by XRD and TEM with the filandrous structure, which was related to the distribution of pores [25]. The bimodal pore size distribution of AE-Cu/SiO_2 catalyst might be attributed to the different silicon species (the filandrous copper phyllosilicate and amorphous SiO_2), while CP-Cu/SiO_2 catalyst had only one pore stemmed from the amorphous SiO_2

because of the weak interaction of copper-silicon.

To gain further investigation for the structure and chemical environment of copper species, we performed Raman technique and the results were showed in Fig. 5. For comparison, three obvious peaks of bulk CuO at 293, 345 and 626 cm^{-1} were observed via the Raman spectra. These characteristic bands of CuO still maintained in CP-Cu/SiO_2 sample, indicating that the copper chemical environment of CP-Cu/SiO_2 sample was similar to that of bulk CuO. That is to say, the interaction of copper-silicon was vitally weak in CP-Cu/SiO_2 catalyst. While the peaks of AE-Cu/SiO_2 catalyst were observed the obvious shift and widened, and it could be clearly observed that AE-Cu/SiO_2 catalyst emerged only one migrated peak at 660 cm^{-1}, indicating that copper species in AE-Cu/SiO_2 catalyst was different with bulk CuO and the conventional CP-Cu/SiO_2 sample.

3.1.3. The chemical environment of the catalysts

In order to further explore the change of copper species in chemical states, H_2-TPR of two Cu/SiO_2 catalysts was performed. As revealed Fig. 6, two Cu/SiO_2 catalysts both presented an asymmetric reduction peak in range of 150-250 °C. Especially, the asymmetric peak of CP-Cu/SiO_2 catalyst shifted toward higher temperature and exhibited broader temperature range than AE-Cu/SiO_2 catalyst. For AE-Cu/SiO_2 catalyst, the peak at lower temperature (210 °C) can be mainly related to the reduction of highly dispersed Cu^{2+} species, and another minor wide peak at 300 °C might be related to the reduction of Cu^{+} species [30]. A.J. Marchi et al. [40] reported that the highly dispersed CuO was reduced at 250 °C, which is more easily reduced than that of bulk CuO. In this work, CP-Cu/SiO_2 catalyst exhibited the higher temperature, which might be chiefly resulted from the reduction of large CuO particles. Therefore, copper species in CP-Cu/SiO_2 catalyst substantially emerged on the formation of large CuO particles, which was probably stemmed from the preparation process [41]. The ammonia evaporation method was beneficial for the formation of Cu nanoparticles, which could help to prevent the fast aggregation of copper particles. In dynamics, the highly dispersed copper particles exhibited the faster reduction than that of bulk CuO [42]. The results of H_2-TPR are consistent with the XRD analysis, indicating that the ammonia evaporation method is propitious to form the highly dispersed Cu nanoparticles.

The surface acidity/basicity plays a critical role in determining the products distribution in furfural hydrogenation [29, 35]. In this work, the surface acidity of samples was investigated through NH_3-TPD experiments. According to Fig. 6, the reduced Cu/SiO_2 catalysts both presented an abroad peak centered at about 190 °C, suggesting that the existence of weak acid sites on two samples. However, the peak area of NH_3 desorption of the reduced AE-Cu/SiO_2 catalyst was much higher than that of CP-Cu/SiO_2 catalyst, indicating that the use of the ammonia evaporation method dramatically improved the surface acid sites of Cu/SiO_2 catalysts. The increase of weak acid sites might be aroused by the special structure of copper phyllosilicate in AE-Cu/SiO_2 sample, which was consistent with that of the calcined catalysts (Fig S2). This special structure would result in the appearance of unsaturated/defective Si^{4+} and Cu^+ species in the catalysts surface [30, 43, 44]. Besides, the production of copper phyllosilicate phase could also enhance the exposure of active copper sites on the surface and strengthen the interaction of copper-silicon [29].

The chemical states of copper were very important for the catalytic performance of catalysts. Especially, the Cu^0 and Cu^+ species of catalysts surface would play the different roles in the catalytic reaction, such as activate the hydrogen and adsorb the groups of substrate [45, 46]. For the conversion of furfural to 2-MF, it need to pass two step reactions of the hydrogenation of side substituents -CH=O groups and the further hydrogenolysis of saturated $-CH_2$-OH groups in Scheme 1, which would refer to the activation of hydrogen and the adsorption of furfural. Thus, we performed the XPS and XAES analysis to discriminate the chemical state of copper, and the results were summarized in Fig. 7 and Fig S3. The XPS spectrum of two Cu/SiO_2 samples after reduction exhibited without Cu 2p peak at 942-944 eV, indicating the disappearance of Cu^{2+} species and the appearance of Cu^0 and Cu^+ species. In order to distinguish Cu^0 and Cu^+ species produced in reduction, the Cu LMM X-ray AES spectrum were performed on these samples and a significant asymmetric peak was observed and overlapped by two peaks at 334.8 and 338.2 eV [45]. The shift of peak at 932.8 and 952 eV was observed on AE-Cu/SiO_2 catalyst in Fig S3, and the overlapping peak of AE-Cu/SiO_2 catalyst shifted to Cu^+ species according to the XAES analysis in Fig. 7. It suggested that the interaction of copper-silicon in AE-Cu/SiO_2 catalyst was assuredly strengthened by the ammonia evaporation method. The enhanced interaction of copper-silicon would be not

advantageous to the reduction of copper species and led to the appearance of Cu^{+} species in the reduction, which is in accordance with the XRD results. The chemical states of copper were greatly affected by the interaction of copper-silicon, which was also authenticated by CO-IR in Fig S4.

For CP-Cu/SiO_2 catalyst, the weak interaction of copper-silicon might be the main reason for the small S_{BET} and the poor copper dispersion. However, AE-Cu/SiO_2 catalyst was composed by the special lamellar structure: the continuous SiO_4 tetrahedra imbedded in the discontinuous CuO_6 octahedra [25]. Therefore, it is easy to understand for the big S_{BET} and the high copper dispersion. Except that, the XRD, TEM and Raman of CP-Cu/SiO_2 sample verified the existence of large CuO particles, which come from the calcination of $Cu_2CO_3(OH)_2$ (Fig. 2A) and formed through the reaction of cupric nitrate and NH_4HCO_3 aqueous solution. Copper species of the calcined AE-Cu/SiO_2 catalyst presented two forms: the major form was a well dispersed Cu-O-Si layer, which was attributed to the competitive reaction of the Cu^{2+} ions with silanol and amino groups by the modulation of pH values [38]. In addition, some weak-bonding copper species dispersed on silicon surface were aggregated to large CuO particles in the calcination [25]. The co-existence of copper phyllosilicate species and a small number of large CuO species in AE-Cu/SiO_2 catalyst aroused the asymmetric peak of H_2-TPR.

3.2 The catalytic performance of Cu/SiO_2 catalysts

3.2.1 The effect of preparation method on the activity and selectivity in furfural hydrogenation.

The catalytic activity of samples was implemented in a fixed-bed reactor. Compared with the conventional catalyst (CP-Cu/SiO_2), AE-Cu/SiO_2 catalyst exhibited the excellence activity, whereas keeping a mild reaction condition in Fig. 8. For CP-Cu/SiO_2 catalyst, furfural conversion was only 63.2% at 140 °C, while AE-Cu/SiO_2 catalyst exhibited the superior catalytic performance at the same temperature, up to a 94.7% furfural conversion. Obviously, the activity of AE-Cu/SiO_2 catalyst was significantly enhanced, especially the activity at low temperature. That is to say, the use of AE-Cu/SiO_2 catalyst would effectively decrease the reaction temperature of furfural hydrogenation to avoid the fast sintering of copper particles at high temperature. On the other hand, 2-MF and FOL selectivity were also exhibited in Fig. 8,

and it was obviously observed that the selectivity of desired product 2-MF over AE-Cu/SiO_2 catalyst was much higher than that of CP-Cu/SiO_2 sample in all the temperature range (140-200 °C). The intermediate FOL was largely obtained over CP-Cu/SiO_2 sample, because the weak acid sites of CP-Cu/SiO_2 sample were shortage and the intermediate FOL could not be converted in further. The results of activity tests clearly confirmed the superior performance of AE-Cu/SiO_2 catalyst for the hydrogenation-deoxygenation of furfural to 2-MF.

Table 2 shows the catalytic performance of AE-Cu/SiO_2 catalyst in furfural hydrogenation as a function of reaction temperature (140-200 °C) under atmospheric pressure. Increasing of reaction temperature evidently improved the overall catalytic performance of furfural hydrogenation. The reaction was very selective to FOL at low temperature (140-160 °C)，while the increase of temperature obviously stimulated the conversion of intermediate FOL to 2-MF, suggesting that the reaction temperature was very significant for the improvement of the desired product 2-MF selectivity. When the reaction temperature increased to 200 °C，an 84.5% yield to 2-MF was obtained over AE-Cu/SiO_2 catalyst. Conversely, the yield of 2-MF was only 47.7% on the conventional CP-Cu/SiO_2 catalyst under the same conditions (Table S1). Evenly, it was observed that 2-MF yield of AE-Cu/SiO_2 catalyst at 180 °C was much higher than that of CP-Cu/SiO_2 catalyst at 200 °C, indicating that the use of AE-Cu/SiO_2 catalyst would decrease at least a 20 °C of reaction temperature to obtain higher yield 2-MF than the conventional CP-Cu/SiO_2 catalyst.

Additionally, weight hourly space velocity (WHSV) is also a vital factor for improving products selectivity [47]. Herein, the effect of WHSV was investigated, and the results were showed in Fig. 9. Interestingly, when the WHSV increased from 0.5 h^{-1} to 2.5 h^{-1}, furfural conversion kept 100% without any decrease, and the selectivity of 2-MF declined only from 95.5% to 83.4% in Fig. 9A. However, the selectivity of 2-MF on CP-Cu/SiO_2 catalyst was greatly influenced by WHSV in Fig. 9B. This phenomenon indicated that the catalytic activity of AE-Cu/SiO_2 sample was excellent, which could obtain much higher 2-MF yield than the conventional CP-Cu/SiO_2 under the same conditions.

For most of Cu-based catalysts, the catalytic performance was closely related to copper species, texture and surface properties of catalyst [34, 48]. Gong et al. [30] proposed that the high copper dispersion was mainly responsible for the good activity in dimethyl oxalate

hydrogenation. Therefore, the increase of copper dispersion (D_{Cu}) was considered as the key reason for the good activity. C. Ciotonea et al. [49] also concluded the highly dispersed nano-phyllosilicate phase was formed via the absorption of mesoporous silica and these metallic nanoparticles apparently exhibited the outstanding activity. In our case, Cu/SiO_2 catalysts were prepared by the different precipitation method, which not only influenced the physicochemical properties of catalysts but also the catalytic performance in furfural hydrogenation. As reported the former literatures [30, 50, 51], the good activity of Cu/SiO_2 catalyst was mainly ascribable to the small particles size, while the poor stability linked the sintering and aggregation of copper species in thermal process. The formation of copper phyllosilicate phase not only decreased the particles size but also strengthened the interaction of copper-silicon, which would change the chemical states of copper and the surface properties of catalyst. AE-Cu/SiO_2 catalyst exhibited the superior activity due to the existence of a large amount of Cu nanoparticles. Moreover, the improvement of 2-MF yield was also associated with the acid sites, and AE-Cu/SiO_2 catalyst afforded the sufficient acid sites and the moderate Cu^+ species, which was propitious to adsorb the reactant furfural on the catalyst surface. Simultaneously, the electrophilic of Cu^+ species could activate -CH=O groups via the lone pair electron of oxygen and considered as Lewis acid sites [52, 53], thus the activity of –CH=O groups in furfural could be promoted. The same electrophilicity of Cu^+ species was also reported for the hydrogenation of crotonaldehyde via Cu-based catalysts [54]. Besides, Dana Procha´zkova et al. [55] and F.V. Mikulec et al. [56] reported that the hydrogenolysis of C-O groups could be promoted by the increase of acid sites and reaction temperature. AE-Cu/SiO_2 catalyst exhibited the superior activity at low temperature, and the reasons were mainly related to the improvement of acid sites and copper dispersion.

3.2.2 The effect of precipitation method on the stability of Cu/SiO_2 catalysts

The long-term performance of CP-Cu/SiO_2 and AE-Cu/SiO_2 catalysts was respectively investigated under a high WHSV (2.0 h^{-1}) and temperature (200 °C). In our previous work [29], CP-Cu/SiO_2 catalyst exhibited the stability of 220 h without the obvious deactivation at a low WHSV (0.5 h^{-1}). However, in this work, the increase of WHSV led to the rapid deactivation of CP-Cu/SiO_2 catalyst, and the results exhibited in Fig. 10. CP-Cu/SiO_2 catalyst presented the

durative decrease of 2-MF selectivity after only 112 h under a big WHSV (2.0 h^{-1}). When the reaction time sustained to 215 h, furfural conversion decreased to 24.4% and the main product was the intermediate FOL on CP-Cu/SiO_2 catalyst. Contrarily, AE-Cu/SiO_2 catalyst could stabilize to 215 h without an obvious deactivation under the identical reaction conditions, and exhibited the superior stability to 2-MF. The good stability of AE-Cu/SiO_2 catalyst might be related to the formation of numerous Cu nanoparticles and the enhanced interaction of copper-silicon, which were favorable to escape the heat and resist the sinter of copper particles.

D. Liu et al. [57] and Camilo I. Meyer et al. [19] reported that the deactivation of Cu-based catalysts was very complex. The chief reasons were proposed such as the deposit of carbon, the aggregation and change of copper species. In this work, it was discovered that the activity of CP-Cu/SiO_2 catalyst obviously decreased after 175 h under a big WHSV (2.0 h^{-1}), and furfural conversion was only 24.4% after reaction 215 h. Thereby, we characterized the spent Cu/SiO_2 catalyst by ICP, TEM and TPR to explore the main reasons of deactivation. For CP-Cu/SiO_2 sample, the results authenticated that it was co-aroused by the severe aggregation and loss of copper species in the reaction process. However, the spent AE-Cu/SiO_2 catalyst did not exhibit the obvious change in copper species.

Copper loading of the fresh CP-Cu/SiO_2 sample is 23.0%, while copper loading of the spent sample is 15.9% according to ICP-OES analysis. This phenomenon indicates the sever loss of copper species in the reaction process. Moreover, the green liquid products after 180 h were discovered the loss of copper components. Furthermore, TEM images of the deactivated sample exhibited much bigger copper particles than the fresh sample in Fig. 11, suggesting the severe aggregation of copper particles in the reaction process. H_2-TPR of the fresh and spent CP-Cu/SiO_2 samples was also showed in Fig S5A, and the spent sample exhibited smaller and broader reduction peak at higher temperature than the fresh sample, which was attributed to the reduction of large copper particles. The severe aggregation and loss of copper species may be caused by the weak interaction of copper-silicon, which is in accordance with the former reports [58, 59]. Especially, the initial decrease of activity on CP-Cu/SiO_2 sample only showed the decrease of 2-MF selectivity without the decline of furfural conversion, indicating the part loss of active sites. After that, the severe deactivation not only exhibited the decrease of 2-MF selectivity, but including the sharp decline of furfural conversion and the main product was the

intermediate FOL. It suggested the severe shortage of active sites, which might be co-aroused by the aggregation and loss of copper species.

However, the spent AE-Cu/SiO_2 sample showed a minor reduction peak at 150 °C, which was assigned to the reduction of passivation layer with 0.5 vol. % O_2/N_2 in Fig. S5B. The stability of catalyst was intimately associated with the interaction of metal-support, and a strong interaction of copper-silicon could effectively retard the transmigration of copper species and improve the lifetime of catalyst [60, 61]. As concluded the former literatures [30, 49], the formation of copper phyllosilicate phase was favorable to provide the stable Cu nanoparticles, which might be in favor of improving the stability of Cu/SiO_2 catalyst. The weak interaction of copper-silicon would lead to the fast deactivation of catalyst due to the easy migration and the accelerated aggregation of copper species in thermal treatment process [62, 63]. Notably, the ammonia evaporation method resulted in the sharp improvement of activity and stability of Cu/SiO_2 catalyst, suggesting a great potential of copper phyllosilicate in the synthesis of 2-MF. Totally, the improved activity and stability of AE-Cu/SiO_2 catalyst was substantially related to be the common contribution of active sites (Cu^0, Cu^+, acid sites) and the enhanced interaction of copper-silicon

4. Conclusion

The different preparation methods greatly influenced the catalytic performance of Cu/SiO_2 catalysts, which was investigated in furfural conversion. The ammonia evaporation method would induce the formation of copper phyllosilicate phase, which could contribute to promote copper dispersion, form the stable Cu nanoparticles and provide the sufficient acid sites. Totally, the yield of 2-MF and the long-term stability were pronouncedly promoted due to the use of AE-Cu/SiO_2 catalyst.

The ammonia evaporation method is advantageous to improve the catalytic performance of Cu/SiO_2 catalyst, and up to the complete conversion with a 95.5% yield to 2-MF at 200 °C, 0.5 h^{-1}. However, CP-Cu/SiO_2 catalyst was prepared by the conventional precipitation, and presented a 77.2% yield of intermediate FOL due to the low copper dispersion and the shortage of acid sites. Detailed characterization revealed that the high copper dispersion and the

enhanced interaction of copper-silicon were predominantly responsible for the outstanding activity and the long-term performance of AE-Cu/SiO_2 catalyst.

Compared with the conventional preparation method, the ammonia evaporation method could effectively decrease the particles size, resist the fast transmigration of copper species in thermal treatment process and improve the catalytic performance of Cu/SiO_2 catalyst. The use of AE-Cu/SiO_2 catalyst could also decrease at least a 20 °C of the reaction temperature in furfural conversion, which is very important for the industrial production of 2-MF. Furthermore, we investigated the deactivation of CP-Cu/SiO_2 catalyst, and it was discovered that the distinct deactivation was co-aroused by the aggregation and loss of copper species.

Acknowledgements

The authors gratefully thank the financial supports of Major State Basic Research Development Program of China (973 Program) (No. 2012CB215305). We would like to thank Dr. Ke Li for the significant help in the experiments.

Reference

[1] J.C. Serrano-Ruiz, R. Luque, A.S. Escribanoa, Chem. Soc. Rev. 40 (2011) 5266-5281.

[2] H. Zhao, J.E. Holladay, H. Brown, Z.C. Zhang, Science. 316 (2007) 1597-1600.

[3] A.J. Ragauskas, C.K. Williams, B.H. Davison, G. Britovsek, J. Cairney, C.A. Eckert, W.J. Frederick Jr, J.P. Hallett, D.J. Leak, C.L. Liotta, J.R. Mielenz, R. Murphy, R. Templer, T. Tschaplinski, Science. 311 (2006) 484-489.

[4] J.J. Bozell, G.R. Petersenb, Green Chem. 12 (2010) 539-554.

[5] J.M. Simmie, J. Wurmel, ChemSusChem. 6 (2013) 36-41.

[6] I.A. Telleria, J. Requies, M.B. Guemez, P.L. Arias, Appl. Catal. B: Environ. 145 (2014) 34-42.

[7] I. A. Telleria, F. Hemmann, C. Jager, P.L. Arias, E. Kemnitz, J. Catal. 305 (2013) 81-91.

[8] G.W. Huber, S. Iborra, A. Corma, Chem. Rev. 106 (2006) 4044-4098.

[9] D.M. Alonso, J.Q. Bond, J.A. Dumesic, Green Chem. 12 (2010) 1493-1513.

[10] Y. Nakagawa, K. Takada, M. Tamura, K. Tomishige, ACS Catal. 4 (2014) 2718-2726.

[11] X. Ma, C. Jiang, H. Xu, H. Ding, S. Shuai, Fuel. 116 (2014) 281-291.

[12] S. Sitthisa, T. Pham, T. Prasomsri, T. Sooknoi, R. G. Mallinson, D. E. Resasco, J. Catal. 280 (2011) 17-27.

[13] S. Sitthisa, D. E. Resasco, Catal. Lett. 141 (2011) 784-791.

[14] A.P. dunlop, Ind. Eng. Chem. 40 (1948) 204-209.

[15] D. Scholz, C. Aellig, I. Hermans, ChemSusChem. 7 (2014) 268 – 275.

[16] K. L. Deutsch, B. H. Shanks, J. Catal. 285 (2012) 235-241.

[17] H. Adkins and R. Connor, J. Am. Chem. Soc. 53 (1931) 1091-1095.

[18] R. Rao, A. Dandekar, R.T.K. Baker, M.A. Vannice, J. Catal. 171 (1997) 406-419.

[19] B.M. Nagaraja, A.H. Padmasri, B. David Raju, K.S. Rama Rao, J. Mol. Catal. A: Chem. 265 (2007) 90-97.

[20] C. I. Meyer, A. J. Marchi, A. Monzon, T. F. Garetto, Appl. Catal. A: Gen. 367 (2009) 122-129.

[21] H. Zheng, J. Yang, Y. Zhu, G. Zhao, React. Kinet. Catal. Lett. 82 (2004) 263-269.

[22] S. Sitthisa, T. Sooknoi, Y. Ma, P. B. Balbuena, D. E. Resasco, J. Catal. 277 (2011) 1-13.

[23] H. Zheng, Y. Zhu, L. Huang, Z. Zeng, H. Wan, Y. Li, Catal. Commun. 9 (2008) 342-348.

[24] K. Xiong, W.S. Lee, A. Bhan, J.G. Chen, ChemSusChem. 7 (2014) 2146-2149.

[25] L. Chen, P. Guo, M. Qiao, S. Yan, H. Li, W. Shen, H. Xua, K. Fan, J. Catal. 257 (2008) 172-180.

[26] Z. Huang, F. Cui, H. Kang, J. Chen, C. Xia, Appl. Catal. A: Gen. 366 (2009) 288-298.

[27] N. Scotti, M. Dangate, A. Gervasini, C. Evangelisti, N. Ravasio, F. Zaccheria, ACS Catal. 4 (2014) 2818-2826.

[28] Z. Wang, Z. Xu, S. Peng, M. Zhang, G. Lu, Q. Chen, Y. Chen, G. Guo, ACS Catal. 5 (2015) 4255-4259.

[29] F. Dong, Y. Zhu, H. Zheng, Y. Zhu, X. Li, Y. Li, J. Mol. Catal. A: Chem. 398 (2015) 140-148.

[30] J. Gong, H. Yue, Y. Zhao, S. Zhao, L. Zhao, J. Lv, S. Wang, X. Ma, J. Am. Chem. Soc. 134 (2012) 13922-13925.

[31] G. Ding, Y. Zhu, H. Zheng, W. Zhang, Y. Li, Catal. Commun. 11 (2010) 1120-1124.

[32] M.Y. Abdul Halim, W.L. Tan, N.H. Hanif Abu Bakar, M.A. Bakar, Materials. 7 (2014)

7737-7751.

[33] C.J.G. van der Grift, P.A. Elberse, A. Mulder, J.W. Geus, Appl. Catal. 59 (1990) 275-289.

[34] A. Gervasini, M. Manzoli, G. Martra, A. Ponti, N. Ravasio, L. Sordelli, F. Zaccheria, J. Phys. Chem. B. 110 (2006) 7851-7861.

[35] S. Sitthisa, W. An, D.E. Resasco, J. Catal. 284 (2011) 90-101.

[36] Z. Huang, F. Cui, H. Kang, J. Chen, X. Zhang, C. Xia, Chem. Mater. 20 (2008) 5090-5099.

[37] F. Boccuzzi, A. Chiorino, G. Martra, M. Gargano, N. Ravasio, B. Carrozziniz, J. Catal. 165 (1997) 129-139.

[38] S. Zhao, H. Yue, Y. Zhao, B. Wang, Y. Geng, J. Lv, S. Wang, J. Gong, X. Ma, J. Catal. 297 (2013) 142-150.

[39] T. Toupance, M. Kermarec, J.F. Lambert, C. Louis, J. Phys. Chem. B. 106 (2002) 2277-2286.

[40] A.J. Marchi, J.L.G. Fierro, J. Santamaria, A. Monzon, Appl. Catal. A: Gen. 142 (1996) 375-386.

[41] L. Trouillet, T. Toupance, F. Villainb, C. Louis, Phys. Chem. Chem. Phys. 2 (2000) 2005-2014.

[42] S. Zhu, X. Gao, Y. Zhu, Y. Zhu, H. Zheng, Y. Li, J. Catal. 303 (2013) 70-79.

[43] D. Barthomeuf, Mater. Chem. Phys. 17 (1987) 49-71.

[44] R.A.van Santen, Studies in Surface Science and Catalysis. 85 (1994) 273-294.

[45] A. Yin, X. Guo, W. Dai, K. Fan, J. Phys. Chem. C. 113 (2009) 11003-11013.

[46] Y. Zhu, X. Kong, S. Zhu, F. Dong, H. Zheng, Y. Zhu, Y. Li, Appl. Catal. B: Environ. 166 (2015) 551-559.

[47] Sreedevi Upadhyayula, J. Chem. Sci. 122 (2010) 613-619.

[48] S. Zhang, G. Fan and, F. Li, Green Chem. 15 (2013) 2389-2393.

[49] C. Ciotonea, B. Dragoi, A. Ungureanu, A. Chirieac, S. Petit, S. Royer, E. Dumitriua, Chem. Commun. 49 (2013) 7665-7667.

[50] A. Dandekar, M. A. Vannice1, J. Catal. 178 (1998) 621-639.

[51] H. Yue, Y. Zhao, L. Zhao, J. Lv, S. Wang, J. Gong, X. Ma, AIChE Journal. 58 (2012) 2798-2809.

[52] M. Boronat, M. May, F. Illas, Sur. Sci. 602 (2008) 3284-3290

[53] A. Dandekar, R. T. K. Baker, M. A. Vannice, J. Catal. 184 (1999) 421-439.

[54] R.M. Rioux, M.A. Vannice, J. Catal. 216 (2003) 362-376

[55] D. Procha´zkova´ , P. Za´mostny´ , M. Bejblova´ , L. erveny´ , J. Cejka, Appl. Catal. A: Gen. 332 (2007) 56-64.

[56] F. V. Mikulec, M. Kuno, M. Bennati, D.A. Hall, R.G. Griffin, M.G. Bawendi, J. Am. Chem. Soc. 122 (2000) 2532-2540

[57] D. Liu, D. Zemlyanov, T. Wu, R.J. Lobo-Lapidus, J.A. Dumesic, J.T. Miller, C.L. Marshall, J. Catal. 299 (2013) 336-345.

[58] M. Montes, J.B. Soupart, M.D. Saeddeleer, B.K. Hodnett, B.Delmon, J. Chem. Soc. 230 (1984) 3209-3220

[59] N. Zhang, Y. Xu, Chem. Materials. 25 (2013) 1979-1988.

[60] L.C.A.van den Oetelaar, A. Partridge, S.L.G. Toussaint, C.F.J. Flipse, H.H. Brongersma, J. Phsy. Chem. B. 102 (1998) 9541-9549.

[61] A. Kumar, Vij. Ramani, ACS Catal. 4 (2014) 1516-1525.

[62] E.S. Vasiliadoua, A.A. Lemonidoua, Appl. Catal. A: Gen. 396 (2011) 177-185.

[63] Z. He, H. Lin, P. He, Y. Yuan, J. Catal. 277 (2011) 54-63.

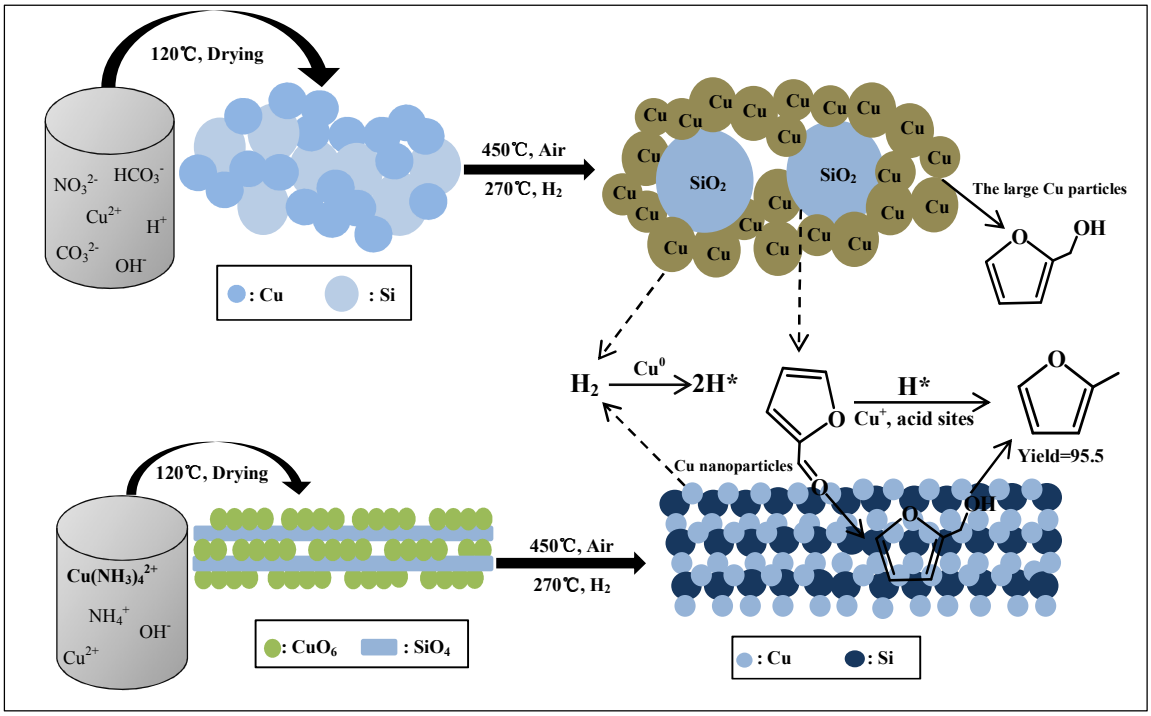

Scheme 1 The Cu/SiO_2 catalysts for the synthesis of biofuel 2-methylfuran through the different preparation methods

Table 1 Physicochemical properties of the different samples

Catalysts	S_{BET} [a] ($m^2 g^{-1}$)	D_{pore} [a] (nm)	V_{pore} [a] ($cm^3 g^{-1}$)	Cu loading [b] (wt.%)		d_{CuO} [c] (nm)	D_{Cu} [d] (%)	S_{Cu} [d] ($m^2 g^{-1}$)	d_{Cu} [e] (nm)	Total acidity [f] (mmol NH_3/g $_{cat}$)
				fresh	spent					
SiO_2	187.1	9.8	0.524	-	-	-	-	-	-	2.09×10^{-2}
CP-Cu/SiO_2	161.4	8.7	0.430	23.0	15.9	8.5	16.8	25.7	16.0	6.61×10^{-2}
AE-Cu/SiO_2	445.1	3.2 6.9	0.759	24.0	23.4	-	22.1	34.9	5.0	13.89×10^{-2}

[a] Determined by N_2-adsorption method, [b] Determined by ICP-OES, [c] Average CuO particle size was calculated by Scherrer equation, [d] Copper dispersion and surface area were determined by N_2O-titration, [e] Average Cu particle size on the reduced samples was determined by TEM, [f] The amount of acid sites was determined by quantifying the desorbed NH_3 from NH_3-TPD.

Table 2 The catalytic performance of AE-Cu/SiO_2 catalyst at the different reaction temperature [a]

T(ºC)	Conversion (%)	Selectivity (%) [b]			
		2-MF	FOL	RO	Others
140	94.7	11.1	88.1	0	0.8
160	95.8	24.4	74.5	0	2.0
180	99.5	56.2	36.6	0.1	7.1
200	100	84.5	2.1	3.4	9.9
200 [c]	96.7	49.4	49.7	0	0.2

[a] Atmospheric pressure, n (H_2/furfural)=17, WHSV=2.0 h^{-1}; [b] 2-MF=2-methylfuran, FOL=furfuryl alcohol, RO=the ring open products(i.e. 2-pentanone, 1-pentanol, 2-pentanol), Others = furan, 2-methyltetrahydrofuran, tetrahydrofurfuryl alcohol, ɤ-valerolactone, furfural polymers; [c] The catalytic performance of CP-Cu/SiO_2 catalyst at 200 °C, n (H_2/furfural)=17, WHSV=2.0 h^{-1}.

Figure Captions

Fig. 1 The curves of pore diameter distribution by BJH equation of A) SiO_2 sample, B) the calcined Cu/SiO_2 samples

Fig. 2 XRD patterns of Cu/SiO_2 catalysts, A) after drying at 120℃; B) after calcination at 450℃; C) after reduction at 270℃

Fig. 3 TEM images of a_1) CP-Cu/SiO_2 sample after drying, a_2) CP-Cu/SiO_2 sample after calcination, a_3) CP-Cu/SiO_2 sample after reduction, b_1) AE-Cu/SiO_2 catalyst after drying, b_2) AE-Cu/SiO_2 sample after calcination, b_3) AE-Cu/SiO_2 sample after reduction; the respective insets are the histograms of Cu particles size distribution (after counting 200 particles)

Fig. 4 FTIR spectra of the calcined Cu/SiO_2 catalysts

Fig. 5 Raman spectra of the calcined Cu/SiO_2 catalysts

Fig. 6 H_2-TPR and NH_3-TPD patterns of Cu/SiO_2 catalysts

Fig. 7 Cu LMM XAES spectra of the reduced Cu/SiO_2 catalysts

Fig. 8 The effect of precipitation method on the activity and selectivity: the black color: CP-Cu/SiO_2 catalyst, the red color: AE-Cu/SiO_2 catalyst, atmospheric pressure, WHSV=2.0 h^{-1}, n (H_2/furfural) =17

Fig. 9 The effect of Weight hourly space velocity: A) AE-Cu/SiO_2 catalyst, B) CP-Cu/SiO_2 catalyst, atmospheric pressure, T=200 °C, n (H_2/furfural) =17

Fig. 10 The stability of Cu/SiO_2 catalysts, atmospheric pressure, T=200 °C, WHSV=2.0 h^{-1}, n (H_2/furfural) =17

Fig. 11 TEM images of CP-Cu/SiO_2 samples before and after reaction: A) the fresh CP-Cu/SiO_2 sample, B) the deactivated CP-Cu/SiO_2 sample; the respective insets are the histograms of Cu particles size distribution (after counting 200 particles)

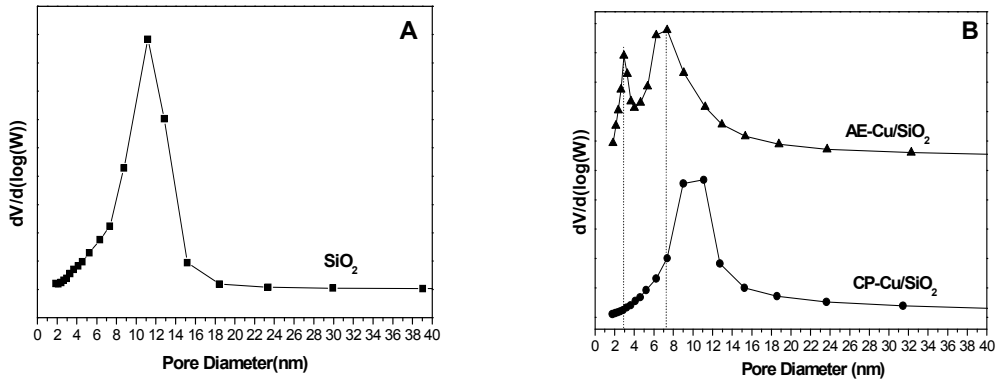

Fig. 1 The curves of pore diameter distribution by BJH equation of A) SiO_2 sample, B) the calcined Cu/SiO_2 samples

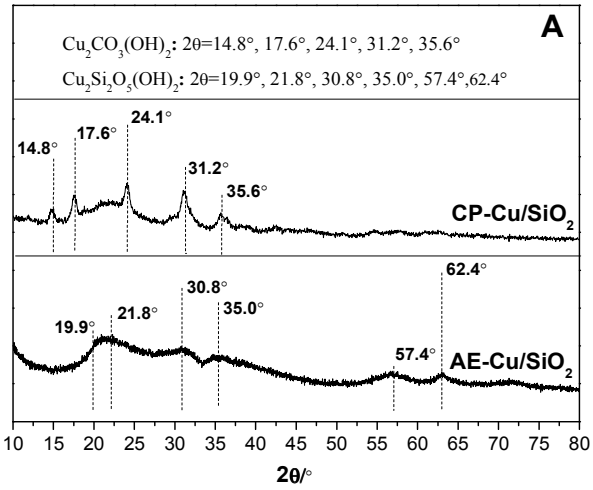

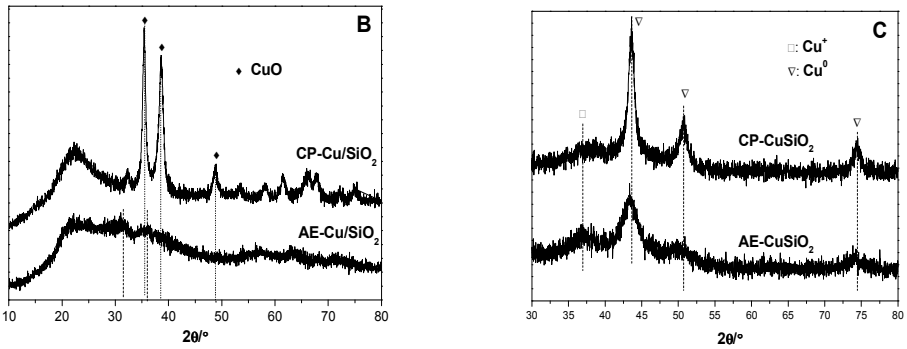

Fig. 2 XRD patterns of Cu/SiO_2 catalysts,
A) after drying at 120℃; B) after calcination at 450℃; C) after reduction at 270℃

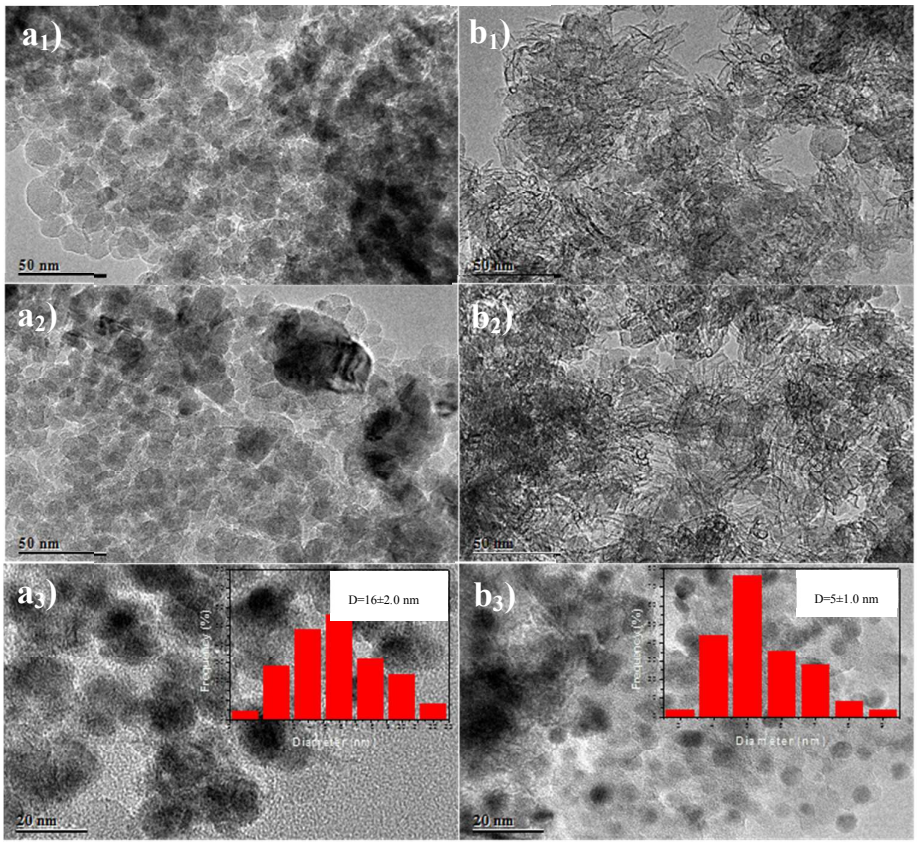

Fig. 3 TEM images of a_1) CP-Cu/SiO_2 sample after drying at 120 °C, a_2) CP-Cu/SiO_2 sample after calcination at 450 °C, a_3) CP-Cu/SiO_2 sample after reduction at 270 °C, b_1) AE-Cu/SiO_2 catalyst after drying at 120 °C, b_2) AE-Cu/SiO_2 sample after calcination at 450 °C, b_3) AE-Cu/SiO_2 sample after reduction at 270 °C; the respective insets are the histograms of Cu particles size distribution (after counting 200 particles).

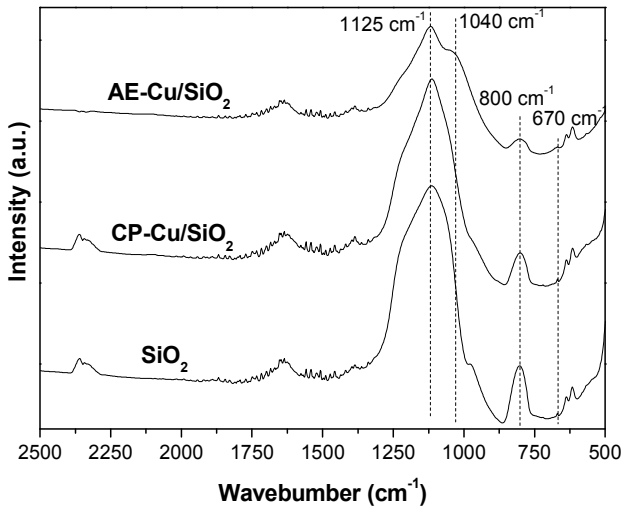

Fig. 4 FTIR spectra of the calcined Cu/SiO_2 catalysts

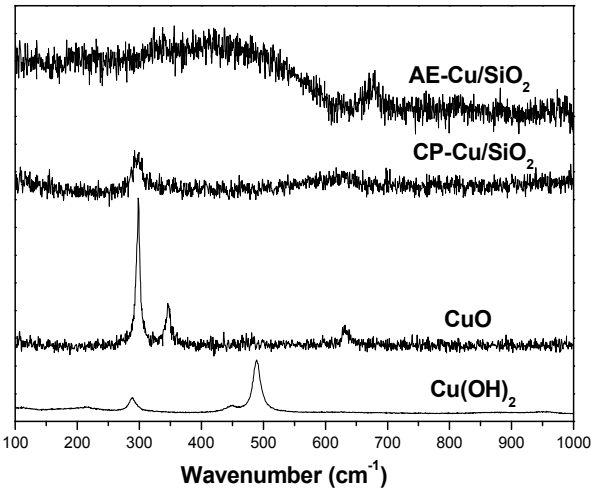

Fig. 5 Raman spectra of the calcined Cu/SiO_2 catalysts

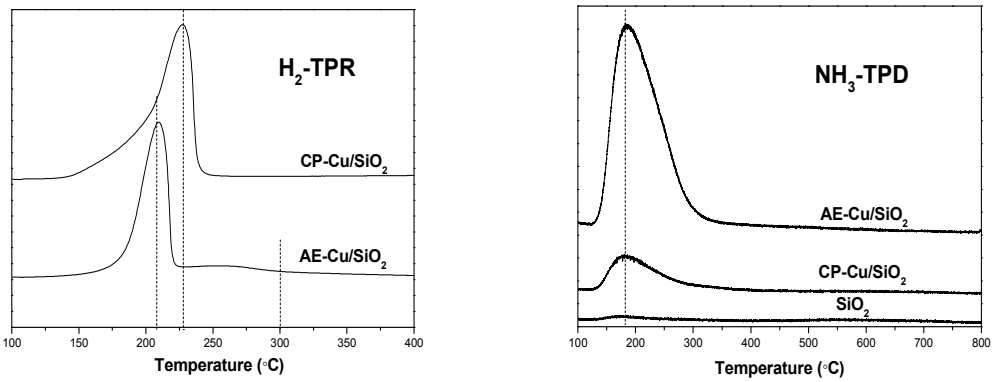

Fig. 6 H_2-TPR and NH_3-TPD patterns of Cu/SiO_2 catalysts

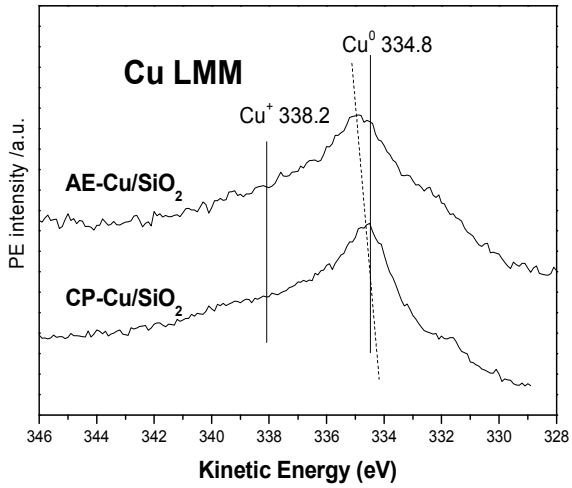

Fig. 7 Cu LMM XAES spectra of the reduced Cu/SiO_2 catalysts

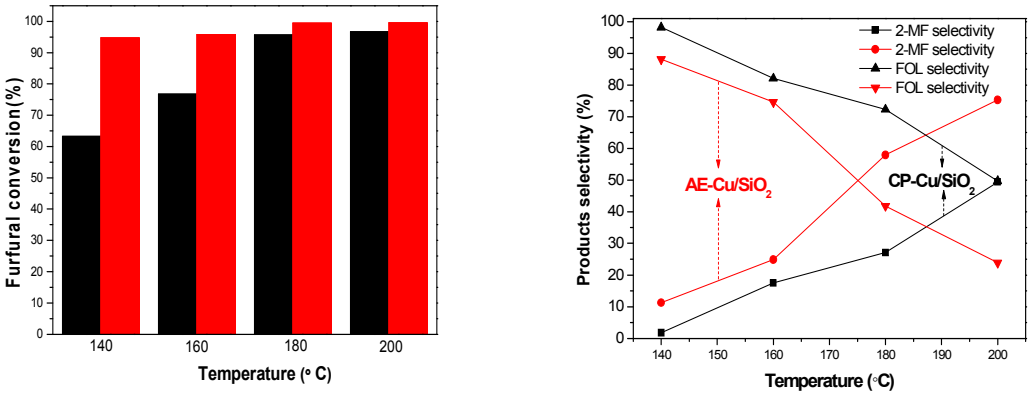

Fig. 8 The effect of precipitation method on the activity and selectivity: the black color: CP-Cu/SiO_2 catalyst, the red color: AE-Cu/SiO_2 catalyst, atmospheric pressure, WHSV=2.0 h^{-1}, n (H_2/furfural) =17

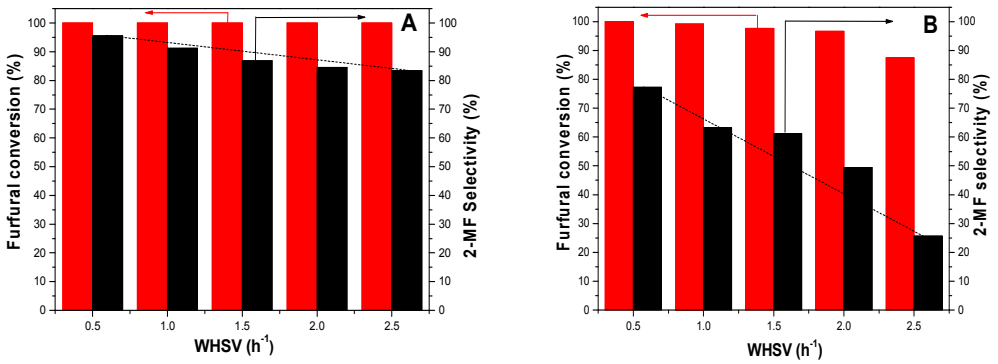

Fig. 9 The effect of Weight hourly space velocity: A) AE-Cu/SiO_2 catalyst, B) CP-Cu/SiO_2 catalyst, atmospheric pressure, T=200 °C, n (H_2/furfural) =17

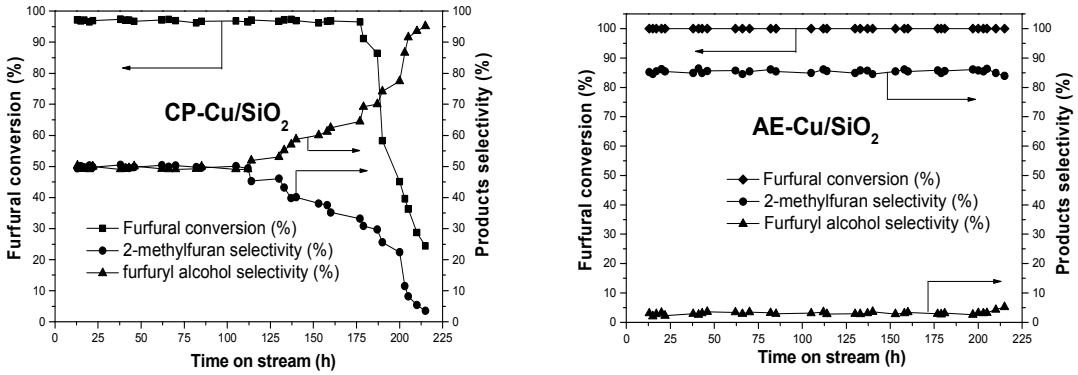

Fig. 10 The stability of Cu/SiO_2 catalysts, atmospheric pressure, T=200 °C, WHSV=2.0 h^{-1}, n (H_2/furfural) =17

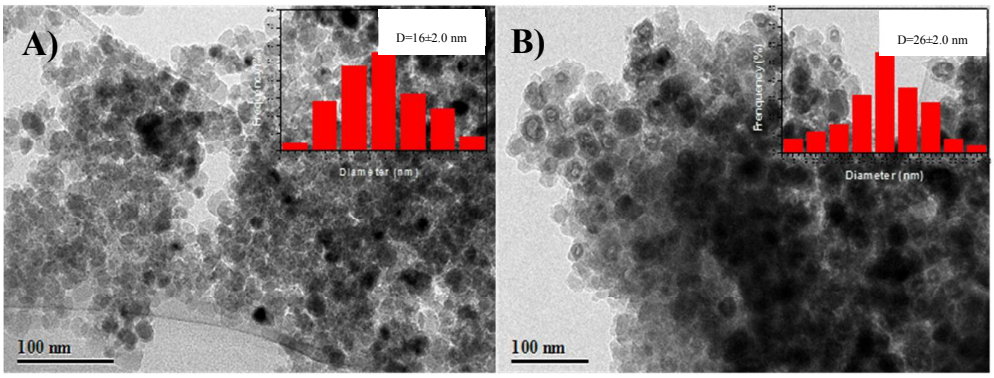

Fig. 11 TEM images of CP-Cu/SiO_2 samples before and after reaction: A) the fresh CP-Cu/SiO_2 sample, B) the deactivated CP-Cu/SiO_2 sample; the respective insets are the histograms of Cu particles size distribution (after counting 200 particles).

A table of contents entry

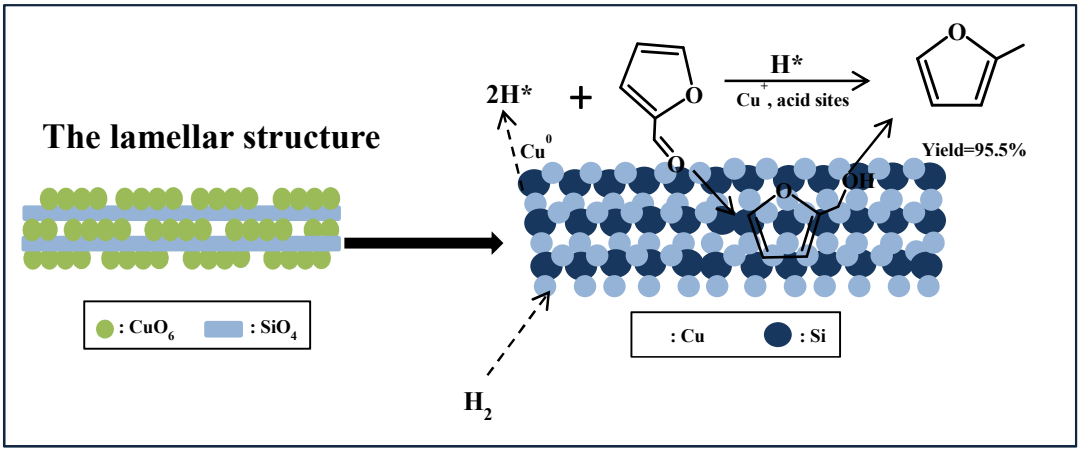

AE-Cu/SiO_2 catalyst obtained a 95.5% yield to 2-methylfuran due to the common contribution of Cu nanoparticles, Cu^+ species and acid sites.